J Mater Sci: Mater Electron (2023) 34:1345

Potentiodynamic electrodeposited M_nO_2:Co_3O_4 thin films electrodes for supercapacitor application

S. V. Khavale[1], R. C. Ambare[2,*], Umesh T. Nakate[3], and B. J. Lokhande[4,*]

[1] Department of Applied Science, Government of Polytechnic, Karad, Maharashtra, India
[2] Department of Physics, K. M. C. College, University of Mumbai, Khopoli 410203, Maharashtra, India
[3] School of Semiconductor and Chemical Engineering, Solar Energy Research Center, Jeonbuk National University, 567 Baekje-Daero, Deokjin-gu, Jeonju-si 54896, Jeollabuk-do, Republic of Korea
[4] Laboratory of Electrochemical Studies, Solapur University, Solapur 413255, Maharashtra, India

Received: 24 November 2022
Accepted: 26 May 2023
Published online: 15 June 2023

ABSTRACT

The existing research explores the effect of annealing temperature on manganese oxide incorporated cobalt oxide thin films synthesized on stainless steel (SS) using potentiodynamic electrodeposition via aqueous route. Film thickness of synthesized material decreases with increase in annealing temperature. Contact angle measurements show decrease in the hydrophilicity with increase in annealing temperature. XRD of the synthesized samples reveals face centered cubic Co_3O_4 and orthorhombic MnO_2 with polycrystalline nature. FESEM and TEM images display nano-spikes with nano-granular morphology. The presence of elemental composition was observed from EDX analysis. The AFM analysis also confirms the nano-granular morphology of fabricated thin film electrodes. The optimized electrodes were investigated for electrochemical characteristics. All CV curves show mixed capacitive behavior. Optimized sample shows maximum specific capacitance (SC) of 605.82 F/g at 2 mV/s using 1 M KOH electrolyte solution. The maximum designed values of energy density, power density and columbic efficiency were 25.20 Wh/kg and 31.10 kW/kg and 92.11% respectively. The observed internal resistance from Nyquist plot (R_i) was 0.64 Ω. The MnO_2 incorporated Co_3O_4 thin films on SS substrates can be a potential candidate for cost-effective supercapacitor applications.

1 Introduction

Now-a-days, whole the world is concerned about increasing environmental pollution, the depletion of fossil fuels and infectivity world which drastically affect socio-ecological systems on the earth. To surmount these problems researchers are developing a battery-supercapacitor hybrid device (BSH) for hybrid electric vehicles. Supercapacitor electrodes are fabricated with various morphologies using a variety

Address correspondence to E-mail: revanambare@gmail.com; bjlokhande@yahoo.com

https://doi.org/10.1007/s10854-023-10718-x

of techniques [1–6]. The transition metal oxides (TMOs), have been proven as suitable electrode materials for pseudo-capacitor [7–10].

Amongst all these TMOs, Co_3O_4 and Mn_3O_4/MnO_2 are easy and economical to prepare, it shows porous morphology, good chemical and physical stability with high specific capacitance [11]. Some researchers have reported porous/3D architecture, nano flowers, nanowires, flakes and spherical grains of Co_3O_4 and Mn_3O_4 using different techniques via aqueous routes [12–20]. Many authors reported the electrochemical measurements of cobalt oxide and manganese oxide synthesized via aqueous route using different methods [21–23]. Some investigators described the electrochemical measurements of manganese oxide prepared via aqueous route using different methods [15, 24, 25].

Pang et al. described the preparation and electrochemical investigation of cobalt oxide–manganese oxide composite which has a maximum specific capacitance (SC) 412 F/g [26]. Jun Chen et al. reported $CoMn(CoMn)_2O_4$ coated on reduced graphene oxide. Corresponding electrode exhibits 571 F/g SC at current density 1 A/g [27]. The details of related literature were studied and the comparison results are reported in Table 1 [28–41]. As per the available literature, there are least evidences found regarding the synthesis of MnO_2:Co_3O_4 thin films by potentiodyanamic electrodeposition and their electrochemical applications which cognate to supercapacitor applications.

The present work focuses on synthesizing manganese incorporated cobalt oxide by potentiodynamic electrodeposition technique and exploring the outcome of annealing temperature on structural, physical and electrochemical parameters. The prepared samples were well characterized using sophisticated tools.

2 Experimental

2.1 Electrodes synthesis

Figure 1 reports details of the synthesis of Mn incorporated cobalt oxide thin films carried out via potentiodynamic electrodeposition technique. Cobalt chloride hexa-hydrate and manganese chloride having AR grade were purchased from Thomas baker chemicals and used without any further purification. 0.1 M solutions of both manganese chloride and cobalt chloride were prepared in double distilled water. The working electrode is 1% Mn incorporated cobalt chloride solution, samples were deposited on SS substrate and counter electrode as a Platinum (Pt) wire and silver/silver chloride as a reference electrode. The potentiostat (CHI 600 D workstation) was used for the potentiodynamic electrodeposition. Deposition was carried out by exploiting cyclic voltammetry range from −1 to −0.1 V with respect to Ag/AgCl reference electrode at the scan rate 80 mV/s for 30 min. As the Annealing temperature is a key factor which may influence structure, morphology, component and mass change of the electrode, the deposited samples were subjected to different annealing temperatures to investigate its effect on crystallinity, surface morphology and electrochemical performance. The different annealing temperatures 473, 523, 573, 623, and 673 K were nomenclature as MAT_1, MAT_2, MAT_3, MAT_4 and MAT_5. The mass loadings for MAT_1- MAT_5 electrodes are 0.0034, 0.00314, 0.00327, 0.00245 and 0.00236 gm respectively and the area of deposited material is 1.5 × 1.5 cm^2. Prepared samples were characterized using XRD, FESEM, EDX, TEM and AFM and cyclic voltammetry to check their structural, morphological and electrochemical properties.

2.2 Characterizations

2.2.1 *Physical characterizations*

The diffractometer of Rigaku D/max 2550 Vb + 18 kW with Cu k_α wavelength was used instrument in the 20°–80° range. Surface studies was done using FESEM (JEOL JSM 7600 FEG-SE). An elemental diffraction analysis (EDX) was carried out using AXFORD-SUK (Japan) at 20 kV to measure the percentage content of manganese incorporated in cobalt oxide. TEM and 2D-AFM images for topographical roughness of prepared samples. The contact angle measurement was carried out using HO-IAD-CAM-01B, Holmark Opto-Mechatronics, India. Tapson-100TS, USA analytical microbalance was used to find the weight of the deposited material.

2.2.2 *Electrochemical characterizations*

The CVs of the prepared electrodes were scanned at room temperature in the potential window −0.95 to

Table 1 Literature reports on manganese incorporated cobalt oxide

R.N	Deposition method	Film properties	Electrolytes/ Scan rate	SC (F/g)	SE (Wh/kg)	SP (kW/kg)	η (%)	Impedance (Hz)
[28]	Chemical co-precipitation Substrate: Ni:Co:Mn = 1:1:1, Was dissolve in 100 ml DW 5% ammonium hydroxide pH = 9.5 vigorous stirring. Potentiodynamic: −0.1 to + 0.45 V/s, scanning rate 5; 10; 20 mV/s, annealing	Mn-Ni-Co oxide	6 M KOH Potential range of − 0.1 to 0.4 V, Scan rate 5 mV/s	1260	–	–	–	10^5 to 10^{-2} Ri = 0.43 Ω
[29]	Potentiostatic deposition Substrate: TiO_2/Ti, HF (3.3)- HNO_3(5.6), At current −1.0 mA/cm^2 for 30 min, 0.02 M $RuCl_3$ and 0.005 M (HCl), scanning rate 10 Potentiodynamic: −0.1 to + 0.6 mV/s, Annealing at 298 K	Co_xNi_{1-x} LDHs Dense microstructure	1 M KOH Scan rate 5 mV/s	2104	–	–	–	0.01to100kHz Ri = 0.05 Ω for Co Ri = 1 Ω for Ni with 45°
[30]	Hydrothermal synthesis Substrate: Nickel foam 5 mmol cobalt acetate, 15 mmol hexamethylenetetramine in 50 ml DW, electrodeposition of Ni 2 mA/cm^2 for 240 s, M $NiCl_2$, 0.05 M, H_3BO_3 and 0.2 M Ethylenediamine dihydrochloride, scanning rate 10 mV/s PD:—0.2 to + 0.6 V	Co $(OH)_2$/Ni	2 M KOH 1 A/g Current density	1310	–	–	–	0.01 Hz to100 kHz
[31]	Electrochemical deposition Substrate: stainless steel Annealed at 300 °C for 3 h PD: −0.7 to + 0 V Ag/AgCl scanning rate 100 mV/s	Co–Ni/Co–Ni Nanocrystalline Cauliflower	1 M KOH Scan rate 1 mV/s	331	–	–	–	Ri = 0.4 Ω
[32]	Chemical precipitation method Substrate: glassy carbon cobalt nitrate + nickel Nitrate(1:1 M), dry at 100 °C, scanning rate 1; 5; 10; 20; 50 mV/s, PD: 0–1.5 V Ag/AgCl	Ni and Co oxide Thin flake	1 M NaOH Scan rate 1 mV/s 0.5 M Na_2SO_4	1840	–	–	–	–
[33]	Hydrothermal method Substrate: Ni foam 200 mg Co (NO_3) in 5 ml 0f DW heated at 180^{0}C for 1.5 h, current densities 0.4 to 3 A/g GS mode	Co_3O_4 @ graphene, nanoflakes	6 M KOH Current density 3 A/g	415	–	–	–	–

Table 1 continued

R.N	Deposition method	Film properties	Electrolytes/ Scan rate	SC (F/g)	SE (Wh/kg)	SP (kW/kg)	η (%)	Impedance (Hz)
[34]	Electrodeposition Nanocrystalline, nano plates PD = −0.2 to 0.6 V	NiCo2O4@NieS	1 M NaOH Current density of 8 mA-cm^{-2}	926	–	–	–	–
[35]	SILAR method SS, 0.1 M $CoSO_4$ and 0.1 M $NiSO_4$ pH − 12, H_2O_2 was kept at 343 K PD: 0 to 500 V	Nickel–cobalt	2MKOH Scan rate 5 mV/s	672	–	–	–	10^{-3} to 10^{3} 0.47 Ω
[36]	Electrodeposition method Ni foams, 0.01 M mixed aqueous solution of $Mn(CH_3COO)_2$ and Na_2SO_4 MnO_2 and MnO_2/reduced graphene oxide (MnO_2/RGO) electrode	MnO_2/RGO	Current density of 5 mA-cm^{-2} 1.0 M Na_2SO_4	343 to 254 to 467 and 307	41.27 Wh/kg to 59.3 Wh/kg	7 KW/kg	–	100,000–0.01
[37]	Electrodeposition method ITO, sodium dodecyl sulfate (SDS) and ethylene glycol (EG) as a templating agent, 10 mM manganese nitrate ($Mn(NO_3)_2$), heated at 200o C for 3 h	Mn_2O_3-SDS + EG	Scan rate 10 mV/s KCl 3 M	72.04	–	–	–	–
[38]	Anodic Electrodeposition nickel foils, Manganese oxide	Manganese oxide nanoflower film and nanowall array,	Current density of 1 mA-cm^{-2}	327	–	–	–	–
[39]	Precipitate 0.005 g $K_3[Co(CN)_6]$, 0.100 g PVP, 10.00 g H_2O and 10.0 ml 10.0 ml 3.3 wt% $Mn(NO_3)_2$, heated at 450 °C	Mn_3O_4–Co_3O_4 cubic-like structured	1.0 M Na_2SO_4 Current density of 12 A/g	289	5.0 Wh/kg	572 W/kg	–	Ri = 1.05 Ω
[40]	Electrodeposition method stainless steel, MnO_2	MnO_2	1.0 M Na_2SO_4 Current density of 2.0 mA cm^{-2}	90–170	–	–	–	–
[41]	Electrodeposition method carbon paper	MnO_2 NF// La_2O_3	Scan rate 5 mV/s 0.5 M Na_2SO_4	–	80.56 Wh/kg	–	–	–
Present work	Electrodeposition method stainless steel, 0.1 M solutions of both manganese chloride and cobalt chloride	MnO_2: Co_3O_4	2 mV/s 1 M KOH	605.82	30 Wh/kg	42.90 kW/kg	95.11	Ri = 0.64 Ω

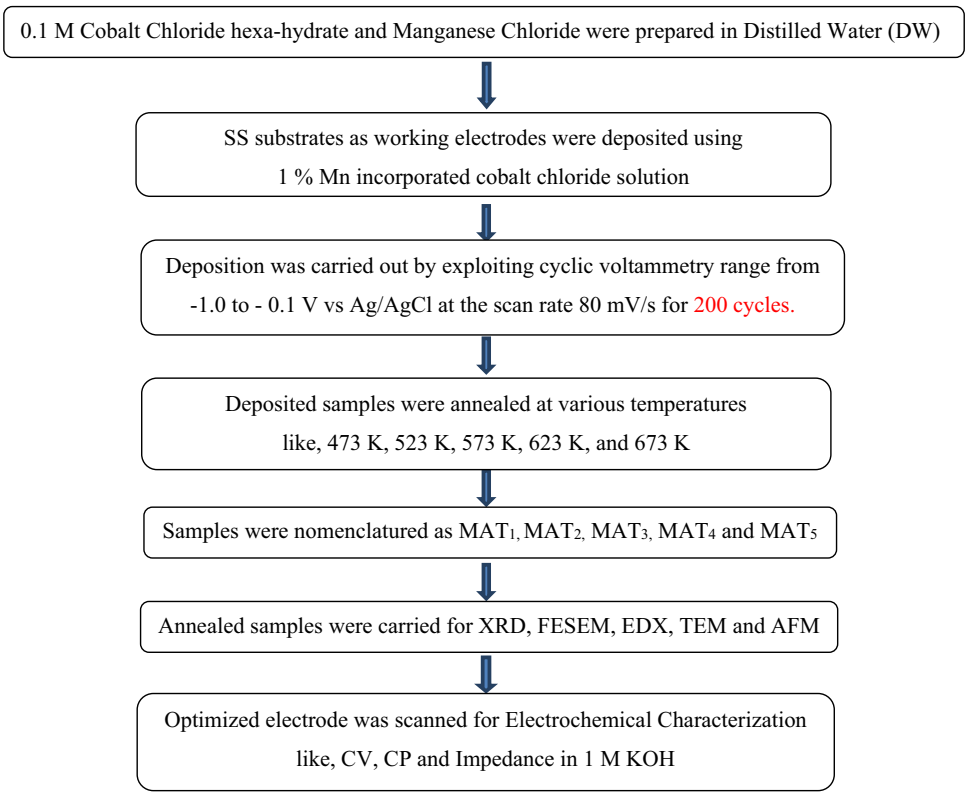

Fig. 1 Flowchart—Thin film deposition and its characterizations

0.48 V Vs silver/silver chloride in 100 mM, 20 ml potassium hydroxide at the scan rate 2 mV/s. The SC of working electrodes was estimated with the assistance of CV [42].

$$SC = \frac{1}{mv(V_c - V_a)} \int_{V_a}^{V_c} I(V)dV \qquad \text{For CV} \qquad (1)$$

$$SC = \frac{I \times t_d}{V \times W} \qquad \text{For CP}$$

where, SC is the specific capacitance, V is the scan rate (mV/s), I represents the current (mA), and 'm' denotes active mass on working electrode, t_d represents discharging time. The energy density, power density and coulombic efficiency (η) were intended.

$$SE = \frac{V \times I_d \times t_d}{W} \qquad (2)$$

$$SP = \frac{V \times I_d}{W} \qquad (3)$$

$$\eta = \frac{t_d}{t_c} \times 100 \qquad (4)$$

Here, 'V' represents voltage, 'I_d' denotes current and 't_d' is discharge time. 'W' is the weight and 't_c' is the charging time.

3 Results and discussion

3.1 Chemical reaction kinetics

The manganese incorporated cobalt oxide thin films were potentio-dynamically electrodeposited at the scan rate 80 mV/s for 30 min. using −1.05 to −0.15 V *Vs* silver/silver chloride deposition window. During the electrodeposition, the cobalt and manganese ions or complexes are hydrolyzed by the distilled water solution to form the hydroxide on the working electrode. After annealing at various temperature (K) for 1.5 h, the $Co(OH)_2$ and $Mn(OH)_2$ was converted into Co_3O_4 and MnO_2 respectively. The possible chemical reactions in the film formation are as given below [43]. After annealing at 473 K $Mn(OH)_2$ gets converted into MnO_2.

$$Mn(OH)_2 + O_2 \longrightarrow MnO_2 + H_2\uparrow + O_2\uparrow \qquad (5)$$

$$3Co(OH)_2 + O_2 \longrightarrow Co_3O_4 + H_2\uparrow \qquad (6)$$

During electrochemical characterizations following reactions may occur

$$3MnO_2 : Co_3O_4 + 6OH^- \leftrightarrow 3Mn : Co(OH)_2 + 5O_2 \uparrow + 6e^- \quad (7)$$

$$Mn : Co(OH)_2 + OH^- \leftrightarrow Mn : CoOOH + H_2O + 1e \quad (8)$$

During electrochemical reaction the nano-composite oxide materials interact with K^+ and OH^- ion and form hydroxide and oxyhydroxide phases during the electrochemical reaction.

3.2 Thickness variation

Thicknesses of the samples were evaluated using gravimetric weight difference method. Figure 2 shows the variation in the film thickness for the samples from MAT_1 to MAT_5. From the figure, it was observed that film thickness decreases with increase in annealing temperature. It may be due to the loss of hydrated content in the film along with an increase in annealing temperature. The similar effect of various temperatures was described for Co_3O_4 thin films synthesized by spray pyrolysis [44].

3.3 XRD studies

Figure 3 XRDs of MAT_1, MAT_2, MAT_3, MAT_4 and MAT_5. The observed '*d*' values were matched with standard '*d*' values taken from JCPDS of Co_3O_4 and MnO_2. All samples are polycrystalline in nature. Co_3O_4 samples exhibit characteristic peaks (220), (311), (400), (331), (440) and (533) at 31.18°, 36.46°, 44.23°, 47.40°, 65.82° and 75.15°. MnO_2, samples exhibit characteristic peaks (101), (201), (210), (211), (202), (331) and (410) at 21.16°, 26.57°, 36.40°, 41.76°, 44.00°, 47.40° and 50.52°. Samples show strong orientations along (400) for Co_3O_4 or (202) for MnO_2 for low temperature annealing and for high temperature annealing, orientations change strongly. Sample MAT_4 shows strong orientation (211) for MnO_2 and sample MAT_5 shows strong orientation (311) for Co_3O_4. The calculated average value of crystallite size '*D*' was around 18 nm for the plane (400) of Co_3O_4/(202) of MnO_2. XRD reveals increase in crystallinity with increase in the annealing temperature. In the fluence of incorporating Mn elements in the Co system may results the more crystalline nature. The similar types of observations were reported for cobalt oxide thin films [45–47]. It may be at high annealing temperature, material gets enough energy to crystallize to orient in proper equilibrium sites, resulting in the upgrade of crystallinity and the degree of direction of the cobalt oxide films [48]. The calculated value of the crystallite size 'D' for plane (400) using Scherer's formula and it is around 21 nm.

3.4 FE-SEM, EDX analysis

Figure 4a depicts FE-SEM images of manganese incorporated cobalt oxide samples annealed at various temperatures. Sample shows porous granular particles along with nano-spikes/nanorods at lower temperature. Inset of the image for sample MAT_1 clearly shows the porous nature of the film at higher magnification. Such morphology possesses high surface area which can be structural base for

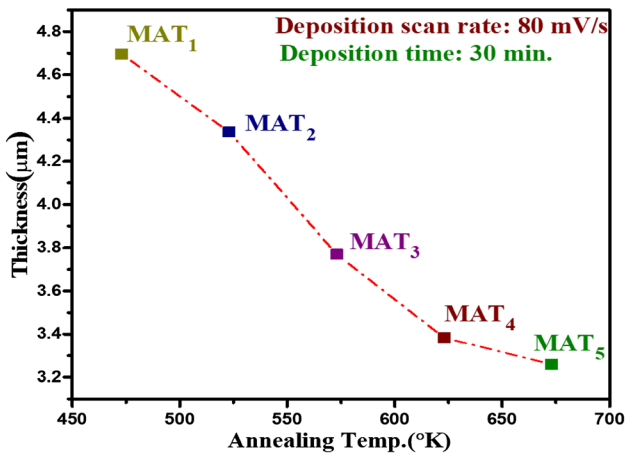

Fig. 2 Variation in thickness with annealing temperature for CM_1 sample

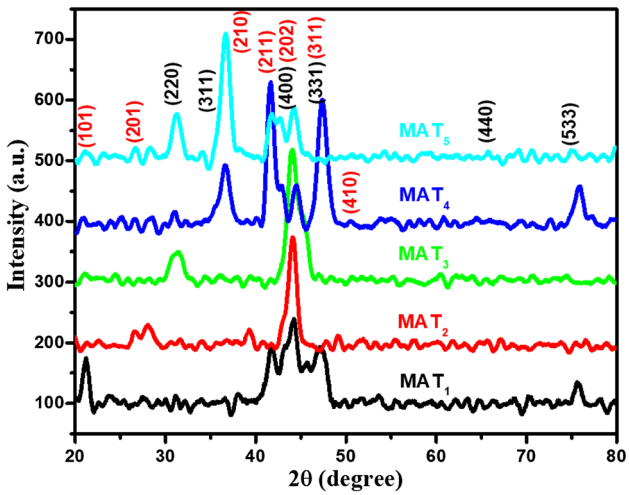

Fig. 3 XRD patterns of the sample CM_1 annealed at different temperatures

electrochemical process [49]. But, with increase in annealing temperature particles are agglomerated to form clusters and nano-spikes/nanorods get disturbed. Porosity of the film drastically gets reduced at higher annealing temperature and it shows compact morphology. The elemental analysis of the MAT_1 sample was carried out by using elemental diffraction analysis. Figure 4b shows the elemental mapping of MAT_1 sample. From the figure it is confirmed that the reported elements are present in the elemental mapping. The contribution of elements for weight percent of Oxygen:18.46; Manganese:1.32; and Cobalt:80.22 and atomic percent contribution are Oxygen:45.44; Manganese:0.95; and Cobalt:53.61 etc.

3.5 TEM, SAED analysis

The micro-structural analysis of MAT_1 electrode was made by using transmission electron microscopy. Figure 5a and b represent as and magnified TEM of MAT_1 sample. It shows formation of granular type of grains corresponding to pure cobalt oxide, along with spikes originated from incorporation of Mn into the pure Co_3O_4 with average spike length $- 3.00 \times 10^2$ nm. Similar nano-spikes/nanorods of MnO_2 were reported by Kim et al. at higher magnifications in cobalt doped manganese oxide thin films [50]. Figure 5c shows the SAED pattern of Mn incorporated Co_3O_4 which confirms crystalline nature of the sample MAT_1.

3.6 AFM analysis

Irregularity of the sample has single importance in the super-capacitive performance as it supports the ion exchange progression (faradaic reaction) in oxide material [51]. Figure 6 depicts 2D AFM micrograph of the sample MAT_1. Micrograph reveals rough agglomerate granular surface morphology with roughness 111 nm. Figure 7.shows contact angle variation for Mn incorporated cobalt oxide thin films annealed at different annealing temperatures. This type of morphological roughness is highly suitable for easy ionic intercalation benefits for better supercapacitive application. The water contact angle depends on the morphology, surface roughness, and chemical properties of the material. In the present case it was observed that contact angle shows decrement in its value and hence decrement the hydrophilicity with increase in annealing temperature. Sample MAT_1 shows super-hydrophilic nature which is feasible for supercapacitor application.

3.7 Electrochemical characterizations

3.7.1 Cyclic voltammetry (CV)

The CV curves for MAT_1 to MAT_5 electrodes were recorded as in Fig. 8a. From the CV curves, it was evidenced that as the annealing temperature increases, the area under CV curves decreases. Change in SC of the different annealed electrodes of MAT_1, MAT_2, MAT_3, MAT_4 and MAT5 were estimated to be 605.82, 431.52, 298.53, 218.36 and 214.58 F/g. The maximum calculated SC of 605.82 F/g was obtained for sample MAT_1 which was decreased to 214.58 F/g for the sample MAT_5. At lower annealing temperature, electrode shows maximum SC, it may be due to easy ionic intercalation. As evident from TEM, influence of MnO_2 impurities *i.e.* porous spikes, hydrophilic nature observed from wettability study may be responsible for increase in surface area responsible to increases the SC as compared to undoped cobalt oxide electrode.

3.7.2 Effect of scan rate

To observe the effect of scan rate on electrochemical performance of the optimized electrode MAT_1, CV was recorded at various scan rates from 2 to 100 mV/s. It was clearly observed that, area under the curve increases with increase in scan rate, at the same time peak was shifted towards negative potential as evidenced from Fig. 8b. The obtained SC values for different scan rates 2, 5, 10, 50 and 100 mV/s are 605.82, 312.09, 308.37, 196.56 and 144.67 F/g. The calculated maximum value of SC was 605.82 F/g at 2 mV/s. As the scan rate increases, SC value decreases. This may be attributed due to the improper ionic intercalation at higher scan rates which affects the charge storing performance of the electrode. At higher scan rates, accessibility of the ions inflowing into all the pores inside the electrode materials rises and thus the transportation of ions was partial due to their slow diffusion. Hence individual the external surface could be exploited for the charge storing [52, 53]. The CV curves of MAT_1 electrode. In both cases it is possible to observe that the presence of redox peaks that can be assigned to

(a)

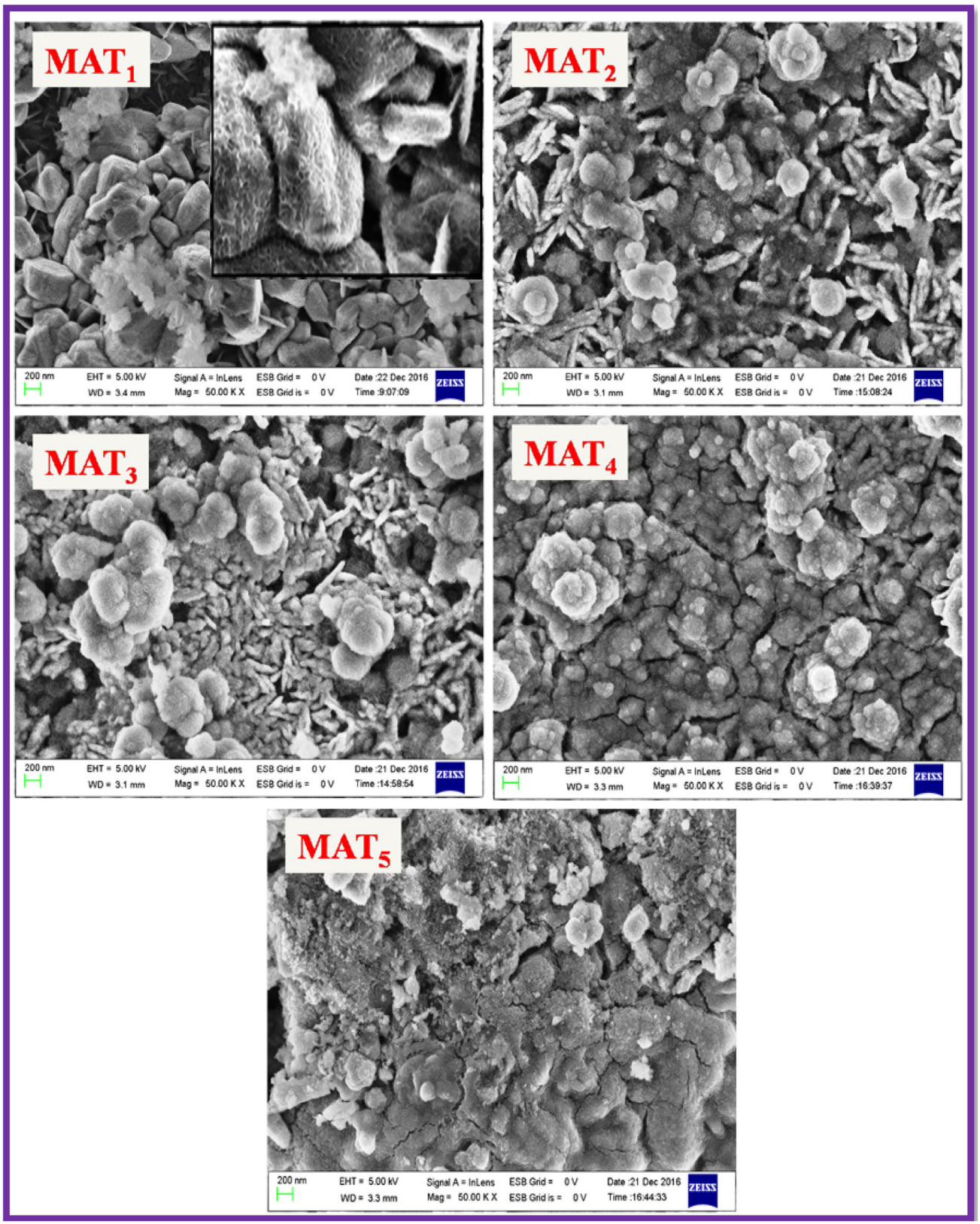
MAT1
200 nm EHT = 5.00 kV WD = 3.4 mm Signal A = InLens Mag = 50.00 K X ESB Grid = 0 V ESB Grid is = 0 V Date :22 Dec 2016 Time :9:07:09 ZEISS
MAT2
200 nm EHT = 5.00 kV WD = 3.1 mm Signal A = InLens Mag = 50.00 K X ESB Grid = 0 V ESB Grid is = 0 V Date :21 Dec 2016 Time :15:08:24 ZEISS
MAT3
200 nm EHT = 5.00 kV WD = 3.1 mm Signal A = InLens Mag = 50.00 K X ESB Grid = 0 V ESB Grid is = 0 V Date :21 Dec 2016 Time :14:58:54 ZEISS
MAT4
200 nm EHT = 5.00 kV WD = 3.3 mm Signal A = InLens Mag = 50.00 K X ESB Grid = 0 V ESB Grid is = 0 V Date :21 Dec 2016 Time :16:39:37 ZEISS
MAT5
200 nm EHT = 5.00 kV WD = 3.3 mm Signal A = InLens Mag = 50.00 K X ESB Grid = 0 V ESB Grid is = 0 V Date :21 Dec 2016 Time :16:44:33 ZEISS

◀**Fig. 4** **a** FESEM images of Mn:Co_3O_4 thin film (CM_1) annealed at different temperatures. **b** Elemental mapping of images for the sample MAT_1 (MAT_1: 1% Mn incorporated Co_3O_4 thin film)

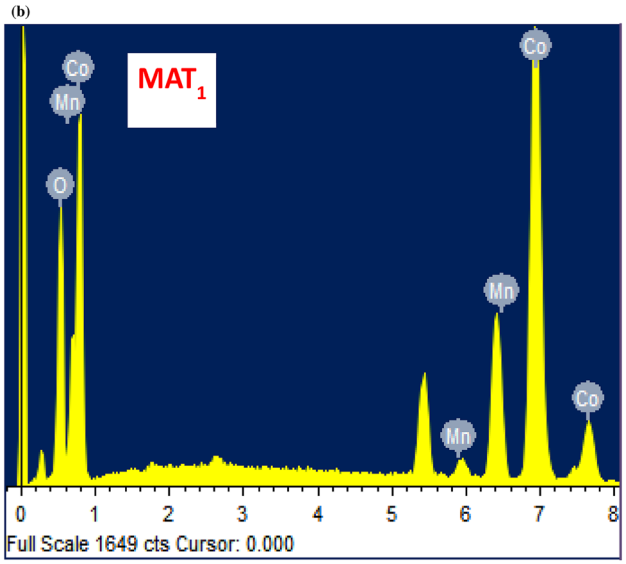

Fig. 4 continued

CoOx-related redox reactions. For MAT_1 electrode the redox peaks can be attributed to the transition Co(II)/Co(III) in the film, which is accompanied by insertion/de-insertion of hydroxyl ions, in order to preserve the electroneutrality of the material during the redox process [54]. It is observed that, with an increase in scan rate from 2 to 100 mV/s, the area under the curve and potential window increases up to − 1.6 V. A reduction reaction must be occurring causes H_2 evolution. A similar result was reported by R. Della Noce et al. [55].

3.7.3 *Effect of electrolytes and electrolytic concentration*

To see the suitability of electrolyte for electrochemical performance, MAT_1 electrode was analyzed in different aqueous inorganic 1 M electrolytes such as KCl, Na_2SO_4 and KOH etc. Figure 8c shows typical CVs of MAT_1 electrode in 1 M solutions of KCl, Na_2SO_4 and KOH respectively. In all electrolytes, electrode shows redox peaks at the particular anodic and cathodic sweeps of CV curves endorses for the mixed-capacitive nature. The calculated values of SC at 2 mV/s in 1 M KOH, Na_2SO_4,and KCl electrolytes are 605.82, 57.56, and 3.66 F/g respectively. Electrode tested in 1 M KOH electrolyte shows maximum SC, which may be attributed due to easy ionic redox activity of aqueous KOH solution with high mobility of K^+/OH^- ions which supports maximum charge storage in the EDL at the electrode—electrolyte boundary and ion diffusion in the host material [22]. One of the most important properties of electrolytic solution is the effective ion size. The size of ions determines the accessibility of the pores to ions and influences on their mobility in the solution bulk. It has been reported [56]. Figure 8d shows the CV curves of MAT_1 electrode carried in different concentrations of KOH. It was evidenced from the area under curve that at lower (less than 1 M) and higher (more than 1 M) concentrations of the electrolyte, capacitive performance was poor. Figure 8e Electrochemical stability curve of MAT_1 electrode scanned in 1 M KOH at 100 mV/s scan rate. Form the figure it is observed that initially the value of SC is 144.67 F/g. With increase in number of cycles for same scan rate current density goes on decrease exponentially. After completion of 2500 number of cycles, the calculated SC is nearly about 140.10 F/g. Further increase in number of cycles the current density and SC associated with materials remains steady. The similar result has been reported [35]. The decrease in SC may be attributed to reduction in pore size and line spacing as evidenced from SEM due to intercalation of potassium ion and showing stable SC beyond 2500 cycles. These results can be due to the different mechanism for storing charge. Assuming that the main storage mechanism for MAT_1 electrode involves bulk redox reactions, the shorter life cycle could be due to irreversible phase changes due to material pseudocapacitive nature that hinder the faradaic process since the continuous $K+/OH-$ insertion/de-insertion will gradually affect the film structure [54].

3.7.4 *Charge–discharge*

Charge–discharge technique is used to understand the energy and power application of the prepared optimized electrode. Figure 9 of MAT_1 electrode scanned at various current densities 10, 15, 20 mA/cm^2 in 1 M KOH. From the figure it is observed that with increase in current density curve shifted towards the triangular side itself indicates the double layer behavior and the prepared electrode material itself indicates the power efficient at higher current density. And at lower current density material shows

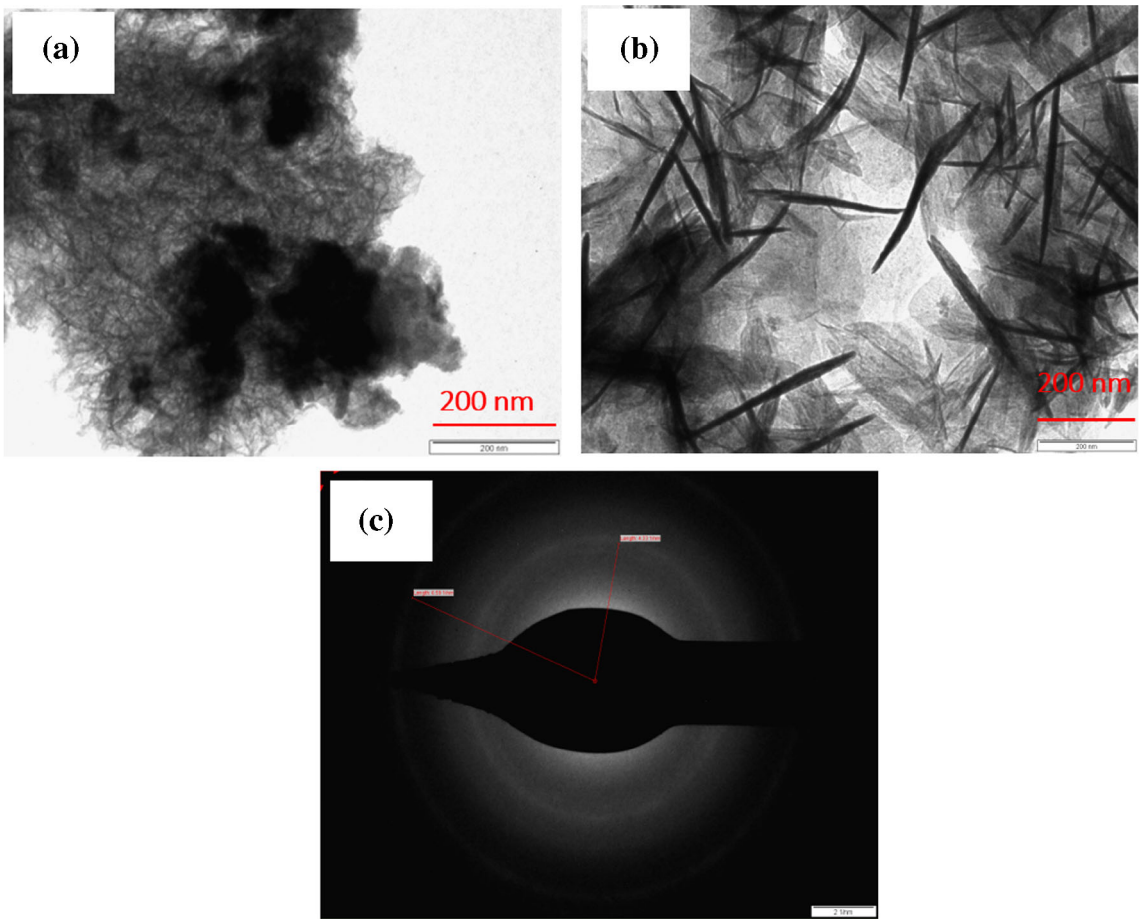

Fig. 5 TEM (**a** and **b**) and SAED (**c**) images for the sample MAT_1 (MAT_1: 1% Mn incorporated Co_3O_4 thin film).

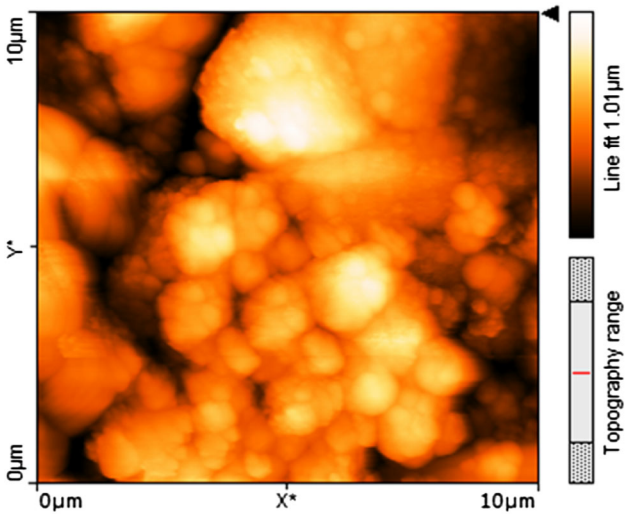

Fig. 6 2D AFM micrograph of MAT_1 sample

pseudocapacitive behavior itself represents energy efficient. The electric parameters associated with MAT_1 electrode was calculated. The SC associated with electrode has been calculated it is − 590.0 F/g at current density 10 mA/cm^2. The maximum calculated values of *SE*, *SP* and η were 25.20 Wh/kg and 31.10 kW/kg and 92.11% respectively.

3.7.5 *Electrochemical impedance*

The internal resistance of MAT_1 electrode was studied using EIS at OCP—0.084103 V in 1 M KOH in the frequency 1 to 1 mHz. Figure 10 shows the Nyquist impedance plot of Z″vs Z′. Nyquist Plot composed of three regions, at maximum frequency region a depressed semicircle results from a parallel combination of the charge-transfer resistance (R_{ct}) produced by the Faradaic reactions at the minimum frequency region. The observed internal resistance (R_i) is 0.64 Ω. The knee frequency (6.21 × 10^{-4} Hz with phase angle 24.4°) which reflect the extreme frequency at which capacitive behavior is govern. Portion of the curve having an inclination of − 45° with Z″ axis gives the value of Warburg resistance

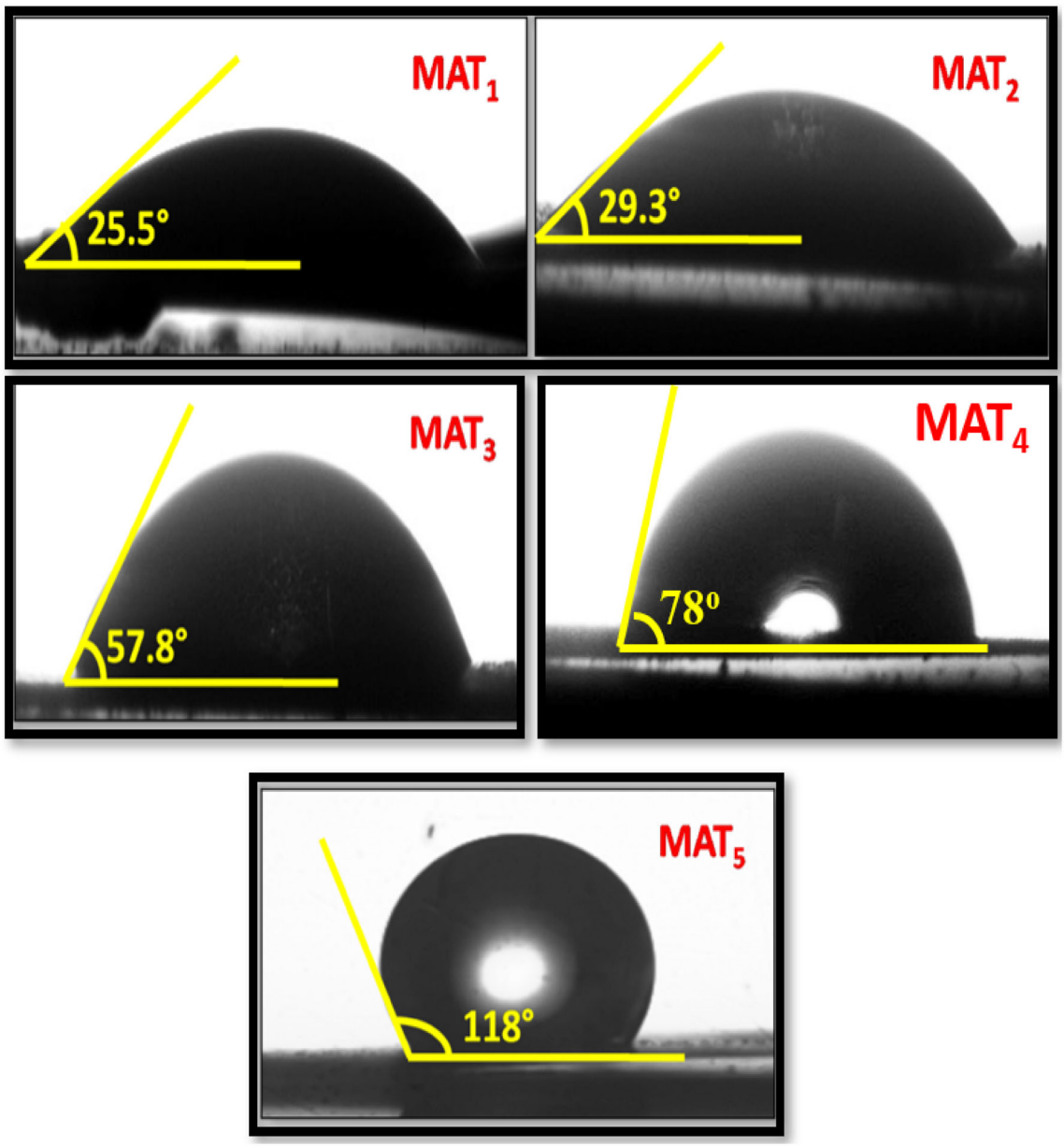

Fig. 7 Wettability images for the Mn:Co_3O_4 thin films annealed at different temperatures

(Z_w). The minimum frequency behavior shifting near 'Y' axis signified double layer capacitance (C_{dl}).

4 Conclusions

Present work reports the successful synthesis of MnO_2 incorporated cobalt oxide electrode using potentiodynamic electrodeposition technique. XRD reveals the FCC and orthorhombic crystal structures for cobalt oxide and manganese oxide respectively. Nano-spike type morphology observed from FESEM. The presence of elemental composition was observed from EDX analysis. TEM study and it signified the incorporation of MnO_2 in cobalt oxide matrix and explored positive effect on the super capacitive effect of Co_3O_4 electrode. Porosity of the film drastically gets reduced at higher annealing temperature implies lower annealing temperature provides excellent capacitive behavior. Optimized electrode scanned in1M KOH electrolyte exhibited high SC 605.82 F/g at 2 mV/s, this specifies capacitive success in contradiction of pristine Co_3O_4 electrode (SC 441.17 F/g). The maximum intended values of SE SP and η were

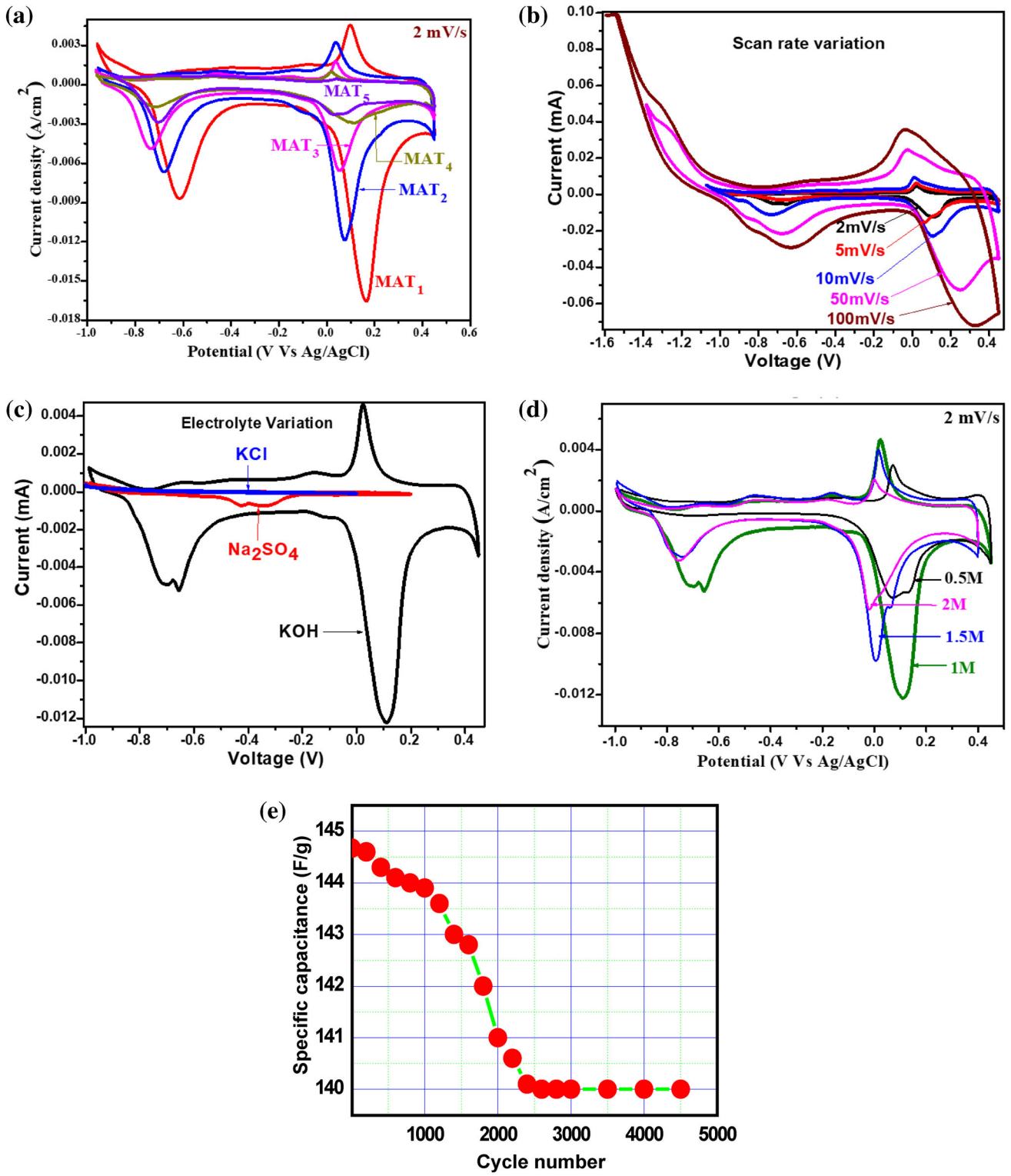

Fig. 8 **a** CVs of CM_1 electrode annealed at different temperatures and scanned in 1 M KOH (CM_1: 1% Mn incorporated cobalt oxide electrode, MAT_1 to MAT_5: 473 K to 673 K with the interval of 50 K), **b** CVs of MAT_1 electrode observed at different scan rates in 1 M KOH (MAT_1: 1% manganese doped Co_3O_4electrode annealed at 473 K), **c** CVs of MAT_1 electrode in different electrolytes (MAT_1: 1%), **d** CVs of MAT_1 electrode observed in different concentrations of KOH. **e** Electrochemical stability curve of MAT_1 electrode scanned in 1 M KOH at 100 mV/s scan rate

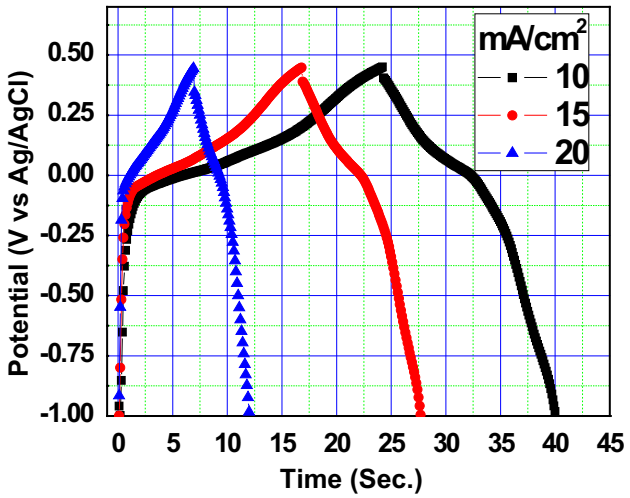

Fig. 9 Charge–discharge curves of MAT_1 electrode scanned at various current densities in 1 M KOH

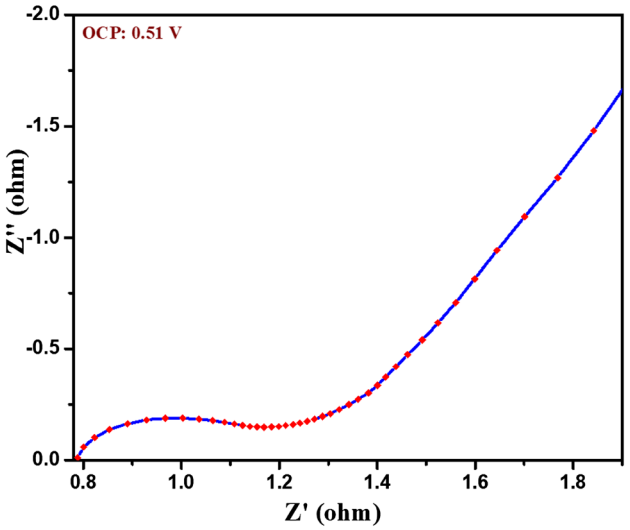

Fig. 10 Nyquist plot of MAT_1 electrode observed in different concentrations of KOH

25.20 Wh/kg and 31.10 kW/kg and 92.11% respectively. The observed internal resistance from Nyquist plot (R_i) is 0.64 Ω. The MnO_2 incorporated Co_3O_4 electrodes have great potential to produce future energy storage devices.

Acknowledgements

Authors are grateful to thanks Department of Science and Technology, New Delhi for providing financial supports through the project scheme DST-SERB sanction no. SB/EMEQ-331/2013.

Author contributions

SVK: Conceptualization, Investigation, Methodology, Writing—review & editing. RCA: Conceptualization, Data curation, Formal analysis, Funding acquisition, Investigation, Methodology, Project administration, Writing—original draft, Writing—review & editing. UTN: Investigation, Formal analysis, Writing—review & editing. BJL: Investigation, Supervision, Writing—original draft, Writing—review & editing.

Funding

The authors have not disclosed any funding.

Data availability

Research data is original and it made available on request.

Declarations

Competing interest The authors declare that they have no known competing financial interests or personal relationships that could have appeared to influence the work reported in this paper.

Ethical approval Indicate that our research manuscript has been conducted ethically, keeping in mind privacy, consent and appropriate reporting of those involved in the study.

References

1. P.R. Deshmukh, N.M. Shinde, S.V. Patil, R.N. Bulakhe, C.D. Lokhande, Supercapacitive behavior of polyaniline thin films deposited on fluorine doped tin oxide (FTO) substrates by microwave-assisted chemical route. Chem. Eng. J. **223**, 572–577 (2013)
2. R. Kotz, M. Carlen, Principles and applications of electrochemical capacitors. Electrochim. Acta **45**(15–16), 2483–2498 (2000)
3. C.N.R. Rao, K. Pramoda, Borocarbonitrides, BxCyNz, 2D nanocomposites with novel properties. Bull. Chem. Soc. Jpn. **92**, 441–468 (2019)
4. U.T. Nakate, P. Patil, S.P. Choudhury, S.N. Kale, Microwave assisted synthesis of Co_3O_4 and NiO nanoplates and

structural, optical, magnetic characterizations. Nano-Struct. Nano-Obj. **14**, 66–72 (2018)
5. W. Wei, X. Cui, W. Chen, D.G. Ivey, Manganese oxide-based materials as electrochemical supercapacitor electrodes. Chem. Soc. Rev. **40**, 1697–1721 (2011)
6. B.E. Conway, *Electrochemical supercapacitors: scientific fundamentals and technological applications* (Kluwer Academic/Plenum Publishers, New York, 1999)
7. P.R. Deshmukh, S.V. Patil, R.N. Bulakhe, S.N. Pusawale, J.-J. Shim, C.D. Lokhande, Chemical synthesis of PANI–TiO_2 composite thin film for supercapacitor application. RSC Adv. **5**, 68939–68946 (2015)
8. M.A. Mahdi, S.R. Yousefi, L.S. Jasim, M. Salavati-Niasari, Green synthesis of $DyBa_2Fe_3O_{7.988}$/$DyFeO_3$ nanocomposites using almond extract with dual eco-friendly applications: photocatalytic and antibacterial activities. Int. J. Hydrogen Energy **47**, 14319–14330 (2022)
9. H. Xia, D. Zhu, Z. Luo, Y. Yu, X. Shi, G. Yuan, J. Xie, Hierarchically structured Co_3O_4@Pt@ MnO_2 nanowire arrays for high-performance supercapacitors. Sci. Rep. **3**, 2978 (2013)
10. H. Jiang, T. Sun, C. Li, J. Ma, Hierarchical porous nanostructures assembled from ultrathin MnO_2 nanoflakes with enhanced supercapacitive performances. J. Mater. Chem. **22**, 2751–2756 (2012)
11. R.C. Ambare, S.R. Bharadwaj, B.J. Lokhande, Spray pyrolysed Mn:Co_3O_4 thin film electrodes via non-aqueous route and their electrochemical parameter measurements. Measurement **88**, 66–76 (2016)
12. J. Xu, L. Gao, J. Cao, W. Wang, Z. Chen, Preparation and electrochemical capacitance of cobalt oxide (Co_3O_4) nanotubes as supercapacitor material. Electrochim. Acta **56**, 732–736 (2010)
13. S. Kumar, G. Saeed, L. Zhu, K. Nam Hui, N.H. Kim, J.H. Lee, 0D to 3D carbon-based networks combined with pseudocapacitive electrode material for high energy density supercapacitor: a review. Chem. Eng. J. **403**, 126352 (2021)
14. T. Yousefi, A.N. Golikand, M.H. Mashhadizadeh, M. Aghazadeh, High temperature and low current density synthesis of Mn_3O_4 porous nano spheres: characterization and electrochemical properties. Curr. Appl. Phys. **12**, 544–549 (2012)
15. S.V. Khavale, B.J. Lokhande, Electrochemical performance of potentio-dynamically deposited Co_3O_4 electrodes: influence of annealing temperature. J. Mater. Sci.: Mater. Electron. **28**, 5106–5115 (2017)
16. X. Cui, F. Hu, W. Wei, W. Chen, Dense and long carbon nanotube arrays decorated with Mn_3O_4 nanoparticles for electrodes of electrochemical supercapacitors. Carbon **49**, 1225–1234 (2011)
17. R.C. Ambare, B.J. Lokhande, Solution concentration and decomposition temperature dependent electrochemical behavior of aqueous route spray pyrolysed Mn_3O_4: supercapacitive approach. J. Mater. Sci.: Mater. Electron. **28**, 12246–12252 (2019)
18. Y.F. Lee, K.H. Chang, C.C. Hu, Y.H. Chu, Designing tuneable microstructures of Mn_3O_4 nanoparticles by using surfactant-assisted dispersion. J. Power Sources **206**, 469 (2012)
19. B. Wang, J. Park, C. Wang, H. Ahn, G. Wang, Mn_3O_4 nanoparticles embedded into graphene nanosheets: preparation, characterization, and electrochemical properties for supercapacitors. Electrochim. Acta **55**(22), 6812–6817 (2010)
20. C.C. Hu, C.Y. Hung, K.H. Chang, Y.L. Yang, A hierarchical nanostructure consisting of amorphous MnO_2, Mn_3O_4 nanocrystallites, and single-crystalline MnOOH nanowires for supercapacitors. J. Power Sources **196**, 847–850 (2011)
21. W. Wei, X. Cui, X. Mao, W. Chen, D.G. Lvey, Morphology evolution in anodically electrodeposited manganese oxide nanostructures for electrochemical supercapacitor applications-effect of supersaturation ratio. Electrochim. Acta **56**, 1619 (2011)
22. R.C. Ambare, S.R. Bhradwaj, B.J. Lokhande, Non-aqueous route spray pyrolyzed Ru:Co_3O_4 thin electrodes for supercapacitor application. Appl. Surf. Sci. **349**, 887–896 (2015)
23. S.R. Yousefi, M. Ghanbari, O. Amiri, Z. Marzhoseyni, P. Mehdizadeh, M. Hajizadeh-Oghaz, M. Salavati-Niasari, Dy_2BaCuO_5/$Ba_4DyCu_3O_{9.09}$ S-scheme heterojunction nanocomposite with enhanced photocatalytic and antibacterial activities. J. Am. Ceram. Soc. **104**, 2952–2965 (2021)
24. S.R. Yousefi, H.A. Alshamsi, O. Amiri, M. Salavati-Niasari, Synthesis, characterization and application of Co/Co_3O_4 nanocomposites as an effective photocatalyst for discoloration of organic dye contaminants in wastewater and antibacterial properties. J. Mol. Liquids **337**, 116405 (2021)
25. R.C. Ambare, S.R. Bharadwaj, B.J. Lokhande, Electrochemical characterization of Mn: Co_3O_4 thin films prepared by spray pyrolysis via aqueous route. Curr. Appl. Phys. **11**, 1582–1590 (2014)
26. H. Pang, J. Deng, J. Du, S. Li, L. Juan, Y. Ma, J. Zhang, J. Chen, Porous nanocubic Mn_3O_4–Co_3O_4 composites and their application as electrochemical supercapacitors. Dal. Trans. **41**, 10175 (2012)
27. J. Chen, Y. Cui, X. Wang, M. Zhi, M. Lavorgna, A.P. Baker, J. Wu, Fabrication of hierarchical porous cobalt manganese spinel graphene hybrid nanoplates for electrochemical supercapacitors. Electrochim. Acta **188**, 704–709 (2016)
28. J.M. Luo, B. Gao, X.G. Zhang, High capacitive performance of nanostructured Mn–Ni–Co oxide composites for supercapacitor. Mater. Res. Bull. **43**, 1125 (2008)

29. V. Gupta, S. Gupta, N. Miura, Potentiostatically deposited nanostructured Co_xNi_{1-x} layered double hydroxides as electrode materials for redox-supercapacitors. J. Power Source **175**, 685 (2008)
30. G.X. Pan, X. Xia, F. Cao, P.S. Tang, H.F. Chen, Porous $Co(OH)_2$/Ni composite nanoflake array for high performance supercapacitors. Electrochim Acta **63**, 340 (2012)
31. V. Gupta, T. Kawaguchi, N. Miura, Synthesis and electrochemical behavior of nanostructured cauliflower-shape Co–Ni/Co–Ni oxides composites. Mater. Res. Bull. **44**, 206 (2009)
32. G. Wang, L. Zhang, J. Kim, J. Zhang, Nickel and cobalt oxide composite as a possible electrode material for electrochemical supercapacitors. J. Power Source **217**, 561 (2011)
33. G. He, J. Li, H. Chen, J. Shi, X. Sun, S. Chen, X. Wang, Hydrothermal preparation of Co_3O_4@graphene nanocomposite for supercapacitor with enhanced capacitive performance. Mater. Lett. **82**, 61–63 (2012)
34. Q. Chu, W. Wang, X. Wang, B. Yang, X. Liu, J. Chen, Hierarchical $NiCo_2O_4$@nickel-sulfide nanoplate arrays for high-performance supercapacitors. J. Power Sources **276**, 19–25 (2015)
35. D.P. Dubal, A.D. Jagadale, S.V. Patil, C.D. Lokhande, Simple route for the synthesis of supercapacitive Co–Ni mixed hydroxide thin films. Mater. Res. Bull. **47**, 1245 (2012)
36. M. Zhang, D. Yanga, J. Li, Effective improvement of electrochemical performance of electrodeposited MnO_2 and MnO_2/reduced graphene oxide supercapacitor materials by alcohol pretreatment. J. Energy Storage **30**, 101511 (2020)
37. D. Lim, T. Park, Y. Choi, E. Oh, S. Shim, S. Baeck, Cathodic electrochemical deposition of highly ordered mesoporous manganese oxide for supercapacitor electrodes via surfactant templating. J. Electrochem. Sci. Technol. **11**(2), 148–154 (2020)
38. H. Fang, L. Zhang, Y. Xing, S. Zhang, S. Wu, Nanostructured manganese oxide films for high performance supercapacitors. Int. J. Electrochem. Sci. **13**, 8736–8744 (2018)
39. H. Pang, J. Deng, J. Du, S. Li, J. Li, Y. Ma, J. Zhang, J. Chen, Porous nanocubic Mn_3O_4–Co_3O_4 composites and their application as electrochemical supercapacitors. Dalton Trans. **41**, 10175–10181 (2012)
40. A. Singh, D. Kumar, A. Thakur, N. Gupta, V. Shinde, B. Saini, R. Kaur, Galvanostatic deposition of manganese oxide films for super capacitive application and their fractal analysis. Ionics **11**, 148–154 (2021)
41. C. Sun, W. Pan, D. Zheng, R. Yao, Y. Zheng, J. Zhu, D. Jia, Low-cost MnO_2 nanoflowers and La_2O_3 nanospheres as efficient electrodes for asymmetric supercapacitors. Energy Fuels **34**, 14882–14892 (2020)
42. R.C. Ambare, P. Shinde, U.T. Nakate, B.J. Lokhande, R.S. Mane, Sprayed bismuth oxide interconnected nanoplates supercapacitor electrode materials. Appl. Surf. Sci. **453**, 214–219 (2018)
43. S.V. Khavale, R.C. Ambare, B.J. Lokhande, Molar optimization of MnO_2 to form composite with Co_3O_4 by potentiodynamic electrodeposition for better electrochemical characterizations. J. Mater. Sci.: Mater. Electro. **31**, 7315–7323 (2019)
44. A. Elsakhi, S.M. Hamed, M.A. Siddig, A.A. Elbadawi, A.I. Mohamed, M.I. Elhadi, Preperation of cobalt oxide thin film using chemical spray pyrolysis method and the effect of annealing temperature in its optical properties. J. Sci. Res. Innov. Tech. **2**, 112–116 (2015)
45. C. Guo, Y. Zhang, M. Yin, J. Shi, W. Zhang, X. Wang, Y. Wu, J. Ma, D. Yuan, C. Jia, Co_3O_4@Co_3S_4 core-shell neuroid network for high cycle-stability hybrid-supercapacitors. J. Pow. Sou. **485**, 229315 (2021)
46. H. Shim, V.R. Shinde, H. Kim, Y. Sung, W. Kim, Porous cobalt oxide thin films from low temperature solution phase synthesis for electrochromic electrode. Thin Solid Films **516**, 8573–8578 (2008)
47. S.R. Yousefi, H.A. Alshamsi, O. Amiri, M. Salavati-Niasari, Synthesis, characterization and application of Co/Co_3O_4 nanocomposites as an effective photocatalyst for discoloration of organic dye contaminants in wastewater and antibacterial properties. J Mol Liquids **337**, 116405 (2021)
48. V.R. Shinde, S.B. Mahadik, T.P. Gujar, C.D. Lokhande, Supercapacitive cobalt oxide (Co_3O_4) thin films by spray pyrolysis. Appl. Surf. Sci. **252**, 7487–7492 (2006)
49. U.M. Patil, K.V. Gurav, V.J. Fulari, C.D. Lokhande, O.S. Joo, Characterization of honeycomb-like "β-$Ni(OH)_2$" thin films synthesized by chemical bath deposition method and their supercapacitor application. J. Power Sources **188**, 338–342 (2009)
50. B. Kim, R.C. Justin, W. Cho, W. Lee, H. Jeong, Y.K. Hyun, Enhanced electrochemical properties of cobalt doped manganese dioxide nanowires. J. Alloys Comp. **617**, 491–497 (2014)
51. Hu. Chi-Chang, T.-W. Tsou, The optimization of specific capacitance of amorphous manganese oxide for electrochemical supercapacitors using experimental strategies. J. Power Sources **115**, 179–186 (2003)
52. V. Srinivasan, J. Weidner, Studies on the capacitance of nickel oxide films: effect of heating temperature and electrolyte concentration. J. Electrochem. Soc. **147**, 880 (2000)
53. R.C. Ambare, S.V. Khavale, U.T. Nakate, M.B. Khanvilkar, B.J. Lokhande, Electrochemical investigations of spray

pyrolysed ruthenium incorporated Co_3O_4 electrodes prepared *via* aqueous route. Colloids Surfaces A **615**, 126215 (2021)
54. A. García-Gómez, S. Eugénioa, R.G. Duarte, T.M. Silva, M.J. Carmezim, M.F. Montemor, Electrodeposited reduced-graphene oxide/cobalt oxide electrodes for charge storage applications. Appl. Surf. Sci. **382**, 34–40 (2016)
55. R. DellaNoce, S. Eugenio, T.M. Silva, M.J. Carmezim, M.F. Montemor, a-$Co(OH)_2$/carbon nanofoam composite as electrochemical capacitor electrode operating at 2 V in aqueous medium. J. Power Sources **288**, 234–242 (2015)
56. K. Torchała, K. Kierzek, J. Machnikowski, Capacitance behavior of KOH activated mesocarbon microbeads in different aqueous electrolytes. Electrochim. Acta **86**, 260–267 (2012)